ELSEVIER

Journal of Biomechanics 37 (2004) 357–366

JOURNAL OF BIOMECHANICS

www.elsevier.com/locate/jbiomech
www.JBiomech.com

# Stresses in the local collagen network of articular cartilage: a poroviscoelastic fibril-reinforced finite element study

W. Wilson[a], C.C. van Donkelaar[a], B. van Rietbergen[a,*], K. Ito[a,b], R. Huiskes[a,c]

[a] *Department of Biomedical Engineering, Eindhoven University of Technology, P.O. Box 513, Eindhoven 5600 MB, Netherlands*
[b] *AO Research Institute, Davos, Switzerland*
[c] *Department of Orthopaedics, University of Maastricht, Netherlands*

Accepted 25 June 2003

**Abstract**

Osteoarthritis (OA) is a multifactorial disease, resulting in diarthrodial joint wear and eventually destruction. Swelling of cartilage, which is proportional to the amount of collagen damage, is an initial event of cartilage degeneration, so damage to the collagen fibril network is likely to be one of the earliest signs of OA cartilage degeneration. We propose that the local stresses and strains in the collagen fibrils, which cause the damage, cannot be determined dependably without taking the local arcade-like collagen-fibril structure into account. We investigate this using a poroviscoelastic fibril-reinforced FEA model. The constitutive fibril properties were determined by fitting numerical data to experimental results of unconfined compression and indentation tests on samples of bovine patellar articular cartilage. It was demonstrated that with this model the stresses and strains in the collagen fibrils can be calculated. It was also exhibited that fibrils with different orientations at the same location can be loaded differently, depending on the local architecture of the collagen network. To the best of our knowledge, the present model is the first that can account for these features. We conclude that the local stresses and strains in the articular cartilage are highly influenced by the local morphology of the collagen-fibril network.


*Keywords:* Cartilage damage; Poroviscoelastic; Finite element analysis; Collagen; Osteoarthritis

## 1. Introduction

Osteoarthritis (OA) is a multifactorial disease, resulting in articular cartilage wear and eventually joint destruction. OA can develop secondary to ultrastructural damage caused by excessive loading. Swelling of cartilage, which is proportional to the amount of collagen damage (Bank et al., 2000), is an initial event of cartilage degeneration (Maroudas, 1976). This suggests that damage to the collagen network is an early event in cartilage degeneration in OA (Pelletier et al., 1983; Verzijl et al., 2002).

The primary collagen fibrils in cartilage extend perpendicular from subchondral bone and gradually curve to a horizontal course, flush with the articular surface, to merge into the surface layer (Benninghoff, 1925; Durham et al., 1988; Clark, 1985, 1991). Since this specialized structure is of essential importance for the mechanical function of cartilage, damage to the collagen network is obviously important for the development of cartilage damage. During excessive impact loading, damage to fibrils in both the superficial layer (Silyn-Roberts and Broom, 1990; Thompson et al., 1991; Atkinson and Haut, 1995; Newberry et al., 1997) and at the cartilage bone interface can occur (Armstrong et al., 1985; Donohue et al., 1983; Thompson et al., 1991; Vener et al., 1992; Atkinson and Haut, 1995). The deformation of the collagen network during loading was studied experimentally by Kääb et al. (1998, 2000) using scanning electron microscopy. They showed that the characteristics of the deformations differ between superficial fibrils and those at the cartilage–bone interface. Using a poroelastic FEA model, we found that superficial damage could only be explained from stress analyses when assuming the cartilage to be anisotropic, but that damage of fibrils at the cartilage–bone interface

*Corresponding author. Tel.: +31-40-247-4773; fax: +31-40-244-7355.
*E-mail address:* b.v.rietbergen@tue.nl (B. van Rietbergen).

0021-9290/$ - see front matter © 2003 Elsevier Ltd. All rights reserved.
doi:10.1016/S0021-9290(03)00267-7

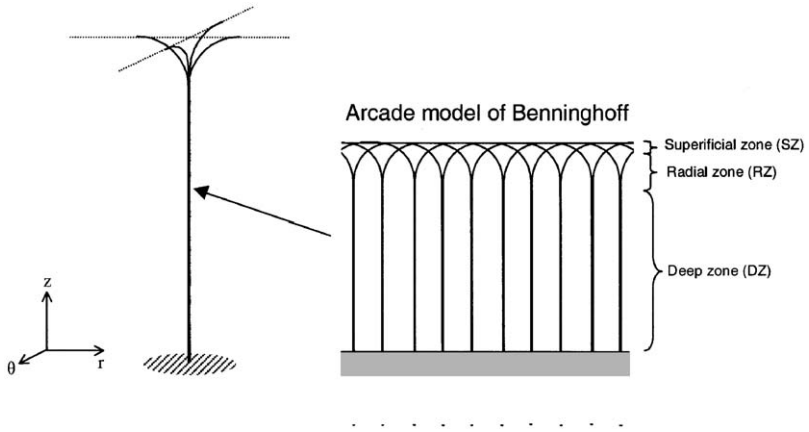


Fig. 1. Orientation of the primary fibrils as a function of depth. Right: cartoon of the arcade model of Benninghoff (1925). Left: Orientation of four primary collagen fibrils as implemented in the FEA model.

can only be predicted in an isotropic model (Wilson et al., 2003). Based on this study we hypothesized that this contradiction could be solved by accounting for the actual, local morphological features of the collagen-fibril network.

Sophisticated FEA models for analyzing cartilage mechanics and the development of damage have been presented (e.g. Atkinson et al., 1997; Garcia et al., 1998; Li et al., 2000, 2002), but only one included a description of collagen fibrils (Li et al., 2000, 2002). This included the collagen fibrils as nonlinear-elastic springs running in axial, radial and circumferential directions. However, this model does not take the specialized architecture of the collagen network into account, nor does it include the viscoelastic properties of the collagen fibrils (Viidik, 1968; Wang et al., 1997; Haut and Little, 1972; Sanjeevi et al., 1982).

In order to test our hypothesis, we developed a poroviscoelastic fibril-reinforced FE model for articular cartilage, which enables the evaluation of stresses and strains in a geometrically realistic arcade-like collagen network. It also includes a secondary fibril network as was observed by Clark (1985, 1991). The constitutive fibril properties were determined by fitting numerical data to experimental results of unconfined compression and indentation tests on samples of bovine patellar articular cartilage (DiSilvestro and Suh, 2001). With our new model we computed the local stresses in different parts of the network.

## 2. Method

Articular cartilage was assumed as biphasic (Mow et al., 1980). The solid matrix consists of a non-fibrillar part of mainly proteoglycans and a fibrillar network of collagen fibrils. In the model, both the non-fibrillar and the fibrillar part of the solid matrix were included in one continuum element.

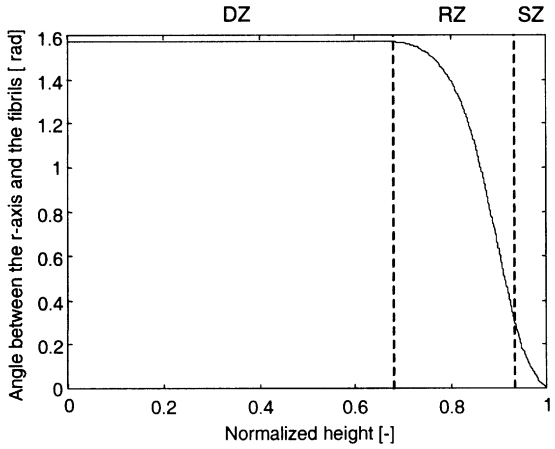


Fig. 2. Angle of the primary collagen fibrils with respect to the *r*-axis.

### 2.1. Fibrillar part

The 3D collagen network was captured as a combination of large primary collagen fibrils and smaller secondary fibrils. As described in the arcade model of Benninghoff (1925), bundles of primary fibrils extend perpendicular from the subchondral bone, splitting up close to the articular surface into fibrils which curve to a horizontal course, flush with the articular surface. Each vertical bundle was assumed to split up in four different fibril directions, curving in radial and circumferential directions (Fig. 1).

In the deep zone, the average angle of the primary fibrils with respect to the *r*-axis as implemented in the FEA model was $\pi/2$. In the radial and superficial zone this angle decreased to become zero at the articular surface (Fig. 2). The thickness of the three zones was obtained from Hunziker (1992). The collagen content is constant in the deep zone, gradually increases in the middle zone, and reaches a total increase of 20% in the superficial zone (Mow and Guo, 2002). To take this into

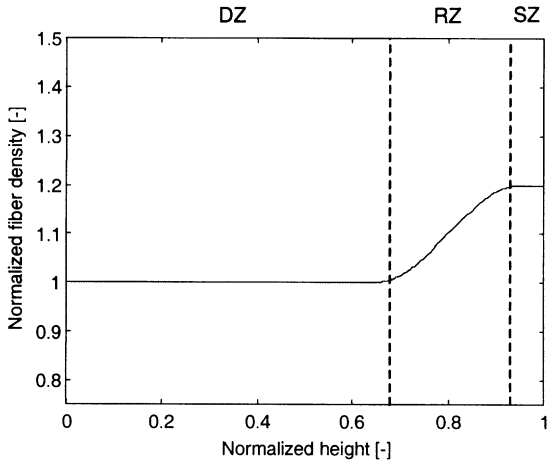


Fig. 3. Relative fibril volume density ($\rho_z$) as a function of depth.

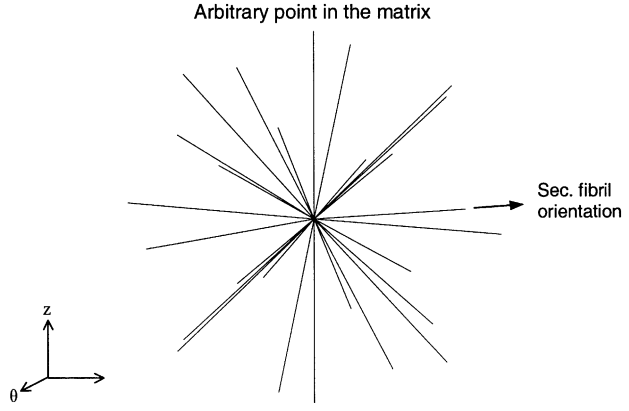


Fig. 4. Schematic representation of the 13 different orientations of the secondary fibrils at any arbitrary point in the matrix.

account, the fibril volume density in the model was made depth dependent (Fig. 3).

It was assumed that orientation of the secondary fibrils is random. The network of secondary fibrils was represented by a homogeneous 3D network of fibrils, running in the $r$-, $\theta$- and $z$-directions, and in all directions with angles of 45° with respect to the $r$-, $\theta$- and $z$-axis (Fig. 4). Hence, the secondary fibrils had 13 different orientations at every integration point. These secondary fibrils are relatively short and account for an extra matrix stiffness in the associated direction.

In the model of Li et al. (2000) the fibril stiffness was given by

$$E_f = E_0 + E_\varepsilon \varepsilon_f, \tag{1}$$

where $E_0$ and $E_\varepsilon$ are positive material constants and $\varepsilon_f$ is the fibril strain. This can be represented as a linear spring with stiffness $E_0$ parallel to a nonlinear spring with stiffness $E_1 = E_\varepsilon \varepsilon_f$ (Fig. 5a). To account for the viscoelastic properties of the collagen fibrils we included a linear dashpot with damping coefficient $\eta$ in series with the non-linear spring (Fig. 5b). This model is similar to

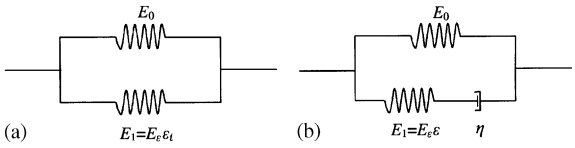


Fig. 5. Schematic models for the elastic collagen fibrils (a) and viscoelastic collagen fibrils (b).

the model of Wang et al. (1997), which was previously used for the description of the viscoelastic behavior of collagen type I. Since there is no dashpot in series with the linear spring, no relaxation of the stresses in the linear spring will occur. Hence, the fibril stresses after full relaxation will be determined by the linear spring. Since the time constant of the spring dashpot model is given by $E_1/\eta$, the relaxation behavior of the fibril is strain dependent. Assuming that the fibrils only resist tension, the stresses in the viscoelastic fibrils are given by

$$\sigma_f = \begin{cases} -\dfrac{\eta}{E_\varepsilon \varepsilon_f}\dot{\sigma}_F + E_0\varepsilon_f + \left(\dfrac{\eta E_0}{E_\varepsilon \varepsilon_f} + \eta\right)\dot{\varepsilon}_f & \text{for } \varepsilon_f > 0, \\ 0 & \text{for } \varepsilon_f \leqslant 0. \end{cases} \tag{2}$$

After time integration with an implicit backward Euler scheme, this becomes

$$\sigma_f^{t+\Delta t} = \begin{cases} -\dfrac{\eta}{E_\varepsilon \varepsilon_f^{t+\Delta t}}\left(\dfrac{\sigma_f^{t+\Delta t} - \sigma_f^t}{\Delta t}\right) + E_0\varepsilon_f^{t+\Delta t} \\ \quad + \left(\dfrac{\eta E_0}{E_\varepsilon \varepsilon_f^{t+\Delta t}} + \eta\right)\left(\dfrac{\varepsilon_f^{t+\Delta t} - \varepsilon_f^t}{\Delta t}\right) & \text{for } \varepsilon_f^{t+\Delta t} > 0, \\ 0 & \text{for } \varepsilon_f^{t+\Delta t} \leqslant 0, \end{cases} \tag{3}$$

where $\sigma_f^{t+\Delta t}$ and $\varepsilon_f^{t+\Delta t}$ are the current fibril stress and strain, respectively, and $\sigma_f^t$ and $\varepsilon_f^t$ the fibril stress and strain from the previous increment. When the depth-dependent fibril density and the relative density between the primary and secondary fibers are taken into account, the stresses in the primary and secondary fibrils are given by

$$\sigma_{f,p} = \rho_z C \sigma_f^{t+\Delta t} \tag{4a}$$

and

$$\sigma_{f,s} = \rho_z \sigma_f^{t+\Delta t}, \tag{4b}$$

respectively. Here $\rho_z$ is a factor accounting for fibril density as a function of depth (Fig. 3), and $C$ the relative density of the primary fibrils with respect to the secondary fibrils.

### 2.2. Non-fibrillar part

The non-fibrillar part of the solid matrix was assumed to be linear elastic, with a Young's modulus $E_m$ and a

Poisson's ratio $\nu_m$. The permeability ($k$) was assumed to be strain dependent (Lai et al., 1981), and is given by (van der Voet, 1997), as

$$k = k_0\left(\frac{1+e}{1+e_0}\right)^M \tag{5}$$

with $k_0$ the initial permeability, $M$ a positive constant, and $e$ and $e_0$ the current and initial void ratios, respectively. The initial void ratio was depth dependent (Li et al., 2000), as

$$e_0 = \hat{e}_0\left(1-\alpha_e\left(1-\frac{z}{h}\right)\right), \tag{6}$$

where $\hat{e}_0$ is the initial void ratio at the articular surface, $\alpha_e$ is a material constant and $h$ is the height of the sample. According to Lipshitz et al. (1975) the water content is about 85% in the superficial layer and decreases to about 70% at the cartilage bone interface. Taken this into account the material constants $\hat{e}_0$ and $\alpha_e$ become 5.667 and 0.413, respectively.

### 2.3. Implementation

At each integration point, the total stress in the solid matrix is given by the sum of the stresses in the non-fibrillar matrix and the sum of all fibril stresses by

$$\boldsymbol{\sigma}_{\text{tot}} = \boldsymbol{\sigma}_{\text{non-fibrillar}} + \sum_{i=1}^{\text{totf}} \boldsymbol{\sigma}^i_{\text{f,global}}, \tag{7}$$

where $\boldsymbol{\sigma}_{\text{non-fibrillar}}$ and $\boldsymbol{\sigma}^i_{\text{f,global}}$ are the stresses in the non-fibrillar matrix and in each individual fibril, both with respect to the global coordinate system. Since the non-fibrillar matrix was assumed to be linear elastic and isotropic, the non-fibrillar matrix stresses can be computed using Hooke's Law. To determine the fibril stresses at each integration point, the initial orientation of each fibril is given by a unit vector ($\vec{v}_0$). After deformation the new unit fibril vector ($\vec{v}_{\text{new}}$) can be computed by

$$\vec{v}_{\text{new}} = \frac{\mathbf{F}\cdot\vec{v}_0}{\|\mathbf{F}\cdot\vec{v}_0\|} \tag{8}$$

with $\mathbf{F}$ the deformation gradient tensor. The logarithmic fibril strain can be computed as

$$\varepsilon_{\text{f}} = \log\|\mathbf{F}\cdot\vec{v}_0\|. \tag{9}$$

With this fibril strain the fibril stresses as given in (4a) and (4b) can be computed. These are longitudinal tensile stresses in the fibrils. By rotating the fibril stresses back to the global coordinate system, the tensile stress in each fibril with respect to the global coordinate system is obtained, as

$$\boldsymbol{\sigma}_{\text{f,global}} = \boldsymbol{\sigma}_{\text{f}}\cdot\vec{v}_{\text{new}}\otimes\vec{v}_{\text{new}}, \tag{10}$$

where $\otimes$ stands for a dyadic product. With the total stress tensor the stiffness tensor can now be computed using (Hibbitt, Karlsson & Sorensen, Inc., 2001)

$$\delta(J\boldsymbol{\sigma}) = J^4\mathbf{C} : \mathbf{D}_\delta, \tag{11}$$

where $J$ is the determinant of the deformation tensor $\mathbf{F}$, ${}^4\mathbf{C}$ the fourth-order stiffness tensor and $\mathbf{D}_\delta$ the virtual rate of deformation, defined as

$$\mathbf{D}_\delta = \text{sym}(\delta\mathbf{F}\cdot\mathbf{F}^{-1}). \tag{12}$$

The model was implemented in ABAQUS v6.2 (Hibbitt, Karlsson & Sorensen, Inc., Pawtucket, RI, USA). The subroutine UMAT was used to define the material behavior of the total solid matrix. An updated Lagrange procedure was used to account for geometric non-linearities that occurred within the model.

### 2.4. Determination of the material properties

The unknown material properties ($E_m$, $\nu_m$, $k_0$, $M$, $E_0$, $E_\varepsilon$, $\eta$ and $C$) were calculated from compression experiments of DiSilvestro and Suh (2001) as described below. DiSilvestro and Suh (2001) performed confined compression, unconfined compression and indentation tests on samples of bovine patellar articular cartilage. It is assumed that the fibrils are not stressed during unconfined compression. Hence, the equilibrium response of the cartilage is determined only by the non-fibrillar part. Therefore, the aggregate modulus of the non-fibrillar part of our model has to be the same as one determined by DiSilvestro and Suh (2001). However, the values for Young's modules $E_m$ and Poisson's ratio $\nu_m$ used by DiSilvestro and Suh (2001) cannot be used directly, because they did not take the equilibrium response of the fibrils into account. Hence, we used a slightly higher Poisson's ratio and a slightly lower Young's modulus compared to DiSilvestro and Suh (2001), which together result in the same aggregate modulus as found by DiSilvestro and Suh (2001). Young's modulus $E_m$ and Poisson's ratio $\nu_m$ of the non-fibrillar part of the solid matrix were set to 0.6228 MPa and 0.15, respectively. The unknown material properties of the fibril-reinforced model are $k_0$, $M$, $E_0$, $E_\varepsilon$, $\eta$ and $C$. These unknown material properties were determined by fitting them to unconfined compression and indentation measurements of DiSilvestro and Suh (2001). We did not use their confined compression results because, according to DiSilvestro and Suh (2001), the boundary conditions for these tests were not trustworthy. The data of DiSilvestro and Suh (2001) included the normalized reaction force of both the unconfined compression and indentation tests and the lateral displacement of the outer edge during the unconfined compression test. The data of DiSilvestro and Suh (2001) were approximated from the graph in their paper with an estimated accuracy of $<1\%$. The fitting procedure itself was performed iteratively using a multidimensional

unconstrained nonlinear minimization procedure available in Matlab Version 5.3 (The MathWorks Inc., 1984–1999). From within this procedure ABAQUS was called to simulate the unconfined compression and indentation tests. The resulting reaction force and lateral displacement data were then transferred into Matlab and normalized in the same way as by DiSilvestro and Suh (2001). In order to be comparable with the single value for the lateral displacement calculated by DiSilvestro and Suh (2001), the lateral displacement was averaged over the height of the sample. For the three data sets the coefficient of determination ($R^2$) were computed. As the objective function, we used

$$f = \sqrt{R^2_{\mathrm{unc,Fr}} + R^2_{\mathrm{ind,Fr}} + R^2_{\mathrm{unc,ul}}}, \tag{12}$$

where $R^2_{\mathrm{unc,Fr}}$ and $R^2_{\mathrm{ind,Fr}}$ are the coefficients of determination of the fits to the reaction force for the unconfined compression and indentation tests, respectively, and $R^2_{\mathrm{unc,ul}}$ is the coefficient of determination of the fit to the lateral displacement for the unconfined compression test. Hence, the model was fitted to the unconfined compression and indentation tests simultaneously.

For the simulation of the unconfined compression test an axisymmetric finite element mesh was used consisting of 750 linear axisymmetric pore pressure elements (CAX4P) (Fig. 6a). The nodal displacements at the bottom plane were confined in the $z$-direction. The displacements of the nodes at the symmetry axis were confined in the $r$-direction. At $r = r_0$, zero pore pressure was prescribed, i.e. fluid can flow in and out freely. The mesh was axially compressed by 10%. After full relaxation, an additional 5% strain at a ramp strain rate of 0.001 $s^{-1}$ was applied. This strain was held constant until full relaxation occurred. While the additional 5% straining and relaxation occurred, axial reaction forces were computed.

For simulation of the indentation test an axisymmetric finite element mesh was used consisting of 600 linear axisymmetric pore pressure elements (CAX4P) (Fig. 6b). The nodes at the bottom plane were confined in all directions. The displacements of the nodes at the symmetry-axis were confined in radial direction. At $z = h$, with $r_{\mathrm{ind}} < r \leqslant r_0$, zero pore pressure was prescribed. At the center, a rigid impermeable indentor with a radius of 1.53 mm was placed on top of the articular cartilage. The indentor was pushed down by applying 10% strain. After full relaxation, an additional 5% strain at a ramp strain rate of 0.001 $s^{-1}$ was applied. This strain was held constant until full relaxation occurred. While the additional 5% straining and relaxation occurred, the axial reaction forces were computed.

## 3. Results

To determine the unknown material parameters of the poroviscoelastic fibril-reinforced FEA model, reaction force and lateral displacements during an unconfined compression and an indentation test as computed with the model were fitted to the experimental data of DiSilvestro and Suh (2001). For the unconfined compression test the FEA reaction force lies well within the experimental range found by DiSilvestro and Suh (2001) (Fig. 7a). The lateral displacement was slightly greater during the loading part compared to the data of DiSilvestro and Suh (2001) (Fig. 7b), but lies well within the experimental range during the relaxation part. For the indentation test, the model described a delayed increase of the reaction force during the loading part, and also a slightly quicker decrease during the relaxation part (Fig. 7c). The coefficients of determination ($R^2$) were 0.94 and 0.85 for the reaction force and lateral displacement in unconfined compression, respectively. The coefficient of determination ($R^2$) was 0.96 for the indentation test. The resulting poroviscoelastic fibril-reinforced model parameters characterizing normal bovine patellar cartilage were determined at $k_0 = 1.743 \times 10^{-15}$ $m^4/N\,s$, $M = 7.081$, $E_0 = 4.735$ MPa, $E_\varepsilon = 490.4$ MPa, $\eta = 1062$ MPa and $C = 12.16$.

To show the importance of accounting for the actual local collagen morphology, the stresses in the primary

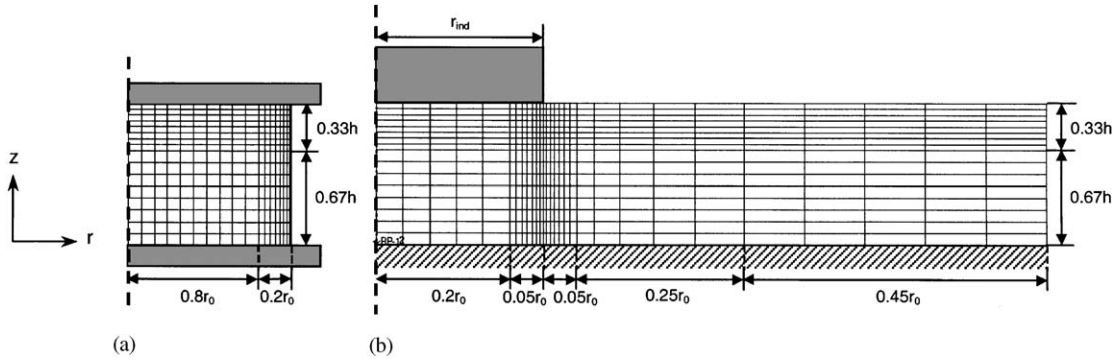


Fig. 6. Scheme of the FEA models used to simulate the tests: (a) unconfined compression mesh ($r_0 = 1.5$ mm, $h = 1.28$ mm), (b) indentation mesh ($r_0 = 6.12$ mm, $r_{\mathrm{ind}} = 1.53$ mm, $h = 1.28$ mm).

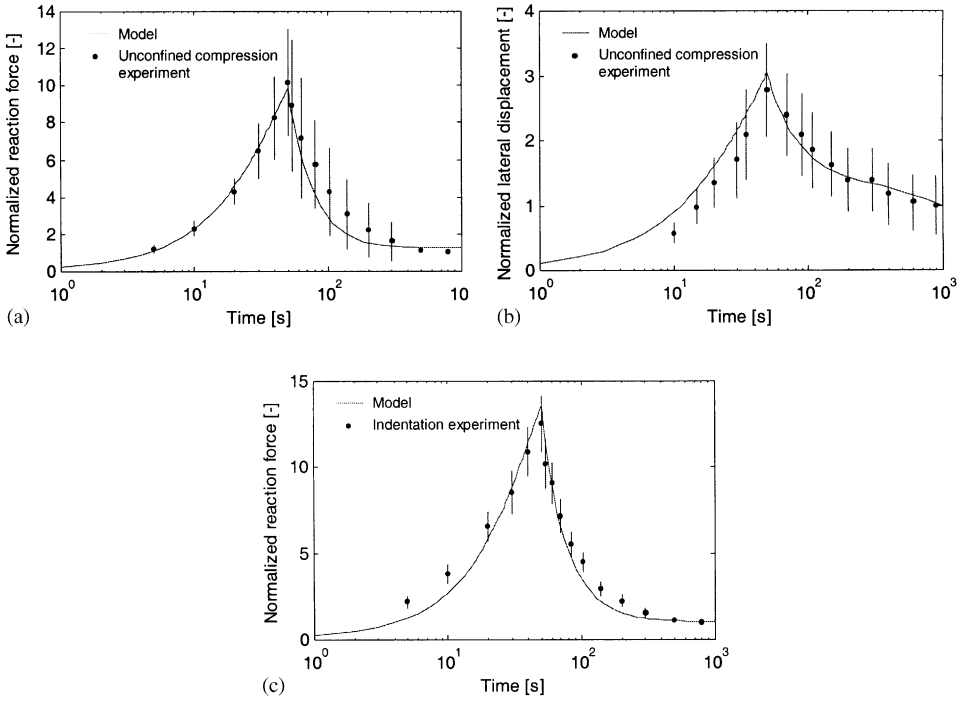


Fig. 7. (a) Axial reaction, force, normalized to equilibrium, measured from unconfined compression tests (DiSilvestro and Suh, 2001) along with fibril reinforced model curve fit. (b) Lateral displacement, measured from unconfined compression tests (DiSilvestro and Suh, 2001) along with fibril reinforced model curve fit. (c) Axial reaction force, normalized to equilibrium, measured from indentation tests (DiSilvestro and Suh, 2001) along with fibril reinforced model curve fit.

fibrils curving towards and away from the center of the joint were plotted for the indentation test (Figs. 8 and 9). Interestingly, there were marked differences between the stresses in the different primary fibrils in the $r$–$z$ plane, depending on the direction of curvature. The fibrils curving away from the center of the joint show peak stresses at the edge of the indentor. This stress peak was absent in the fibrils curving towards the center of the joint. This can be explained by considering that the fibrils only resist tension and by the fibril deformations (Figs. 8 and 9). The fibrils curving away from the center of the joint bend toward the direction of maximal strain, and hence are strained. Whereas the fibrils that curve towards the center bend away from the direction of maximal strain, and hence are not strained.

## 4. Discussion

The FE model presented in this paper incorporates the ultrastructural 3D architecture of viscoelastic collagen fibrils, observed experimentally, into a poroviscoelastic fibril-reinforced material model of articular cartilage. For this new approach, a new set of material parameters had to be defined and their values determined. Some of these were taken directly from the literature, while others were calculated from fits to published experimental data. With this model the reaction force during indentation and unconfined compression as well as the lateral deformation during unconfined compression could be accounted for simultaneously. Until now this was only possible with the poroviscoelastic model of DiSilvestro and Suh (2001). DiSilvestro's model can only simulate bulk behavior, and does not take the behavior of the collagen network into account.

The values found for the permeability $k_0$ and the constant $M$ correspond well with those found in the literature (Hasler et al., 1999; Spilker et al., 1988). The values found for $E_0$ and $E_\varepsilon$ are one order of magnitude lower than those of Li et al. (1999, 2000, 2002). This is due to the fact that the fibril density in our model is higher and that the fibril architecture has been taken into account. These differences might also be partially caused by the real differences in material properties between patellar and humeral cartilage. The ratio between $E_0$ and $E_\varepsilon$ was similar to the one in Li et al. (1999, 2000, 2002). For the damping coefficient $\eta$ no literature data is available. However, the relaxation time of the collagen fibrils was very similar to the one found by Wang et al. (1997) for collagen type I.

For the relative density between the primary and secondary fibrils ($C$) no literature date are available. It should be noted that the number of different primary and secondary fibrils in each integration point was 4 and 13, respectively. Hence, the actual relative density is $12.16 \times \frac{4}{13} = 3.74$. A sensitivity analysis showed that the relative density between the primary and secondary

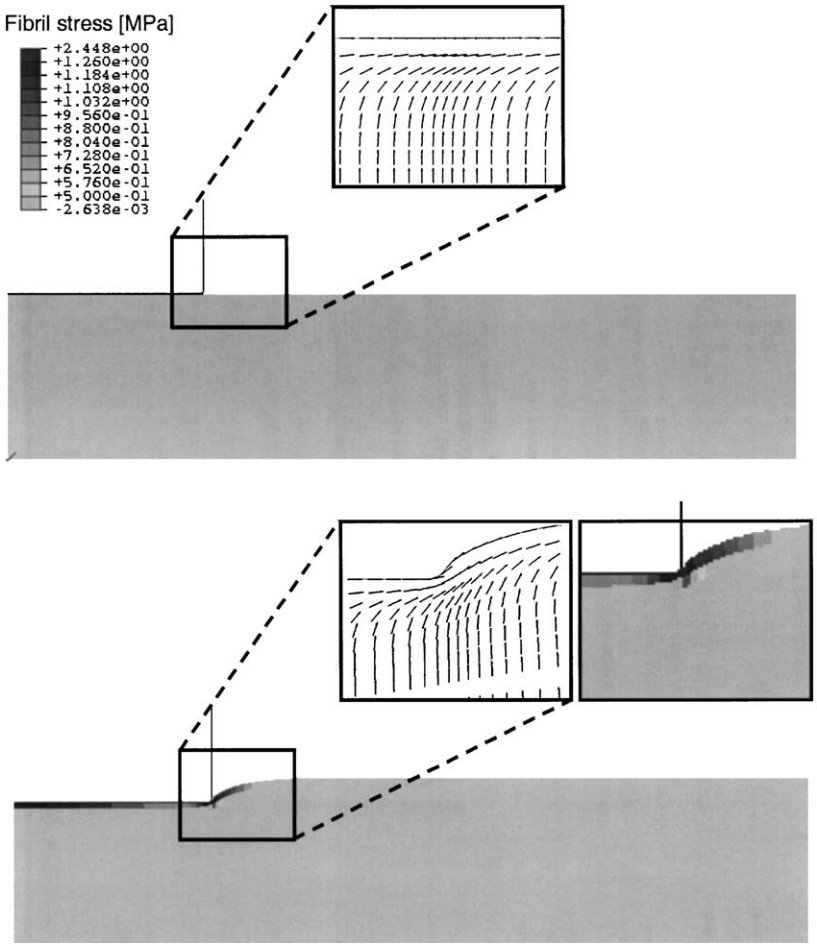


Fig. 8. Contour plot of the fibril stresses in the primary fibrils curving away from the center of the joint at $t = 50$ s, along with the fibril directions around the edge of the indentor. At the top the unloaded state is shown and at the bottom the state at $t = 50$ s.

fibrils only slightly influenced the unconfined compression test. During this test the deformation throughout the tissue is more or less equal. Since the secondary fibril network is also homogeneous, the properties of this network mainly determine the overall behavior of the tissue. During indentation, however, the superficial cartilage layer is stretched horizontally, while the deep zone is stretched vertically. Hence, predominant straining throughout the height of the tissue is in the direction of the primary fibrils and therefore the primary fibrils are dominant. Thus, the indentation test was very sensitive to the value of $C$.

When fitting multiple material parameters it is always the question whether a unique fit has been obtained. In our model each material parameters had a distinct and different influence on the mechanical response. Furthermore, the fit was performed with different initial values for each parameter, and all fits resulted in the same values. Hence, we believe that it is very likely that a unique fit has been obtained. Moreover, the parameter values correspond with those determined by others.

It is known that the non-fibrillar part of the solid matrix has depth-dependent (Schinagl et al., 1997) and viscoelastic properties (Mak, 1986). It is also known that chemical interactions play a role in the mechanical behavior of articular cartilage (Lai et al., 1991). However, these features have not been included in our model, which could explain some of the mismatches of the model compared with experimental data. However, this was not investigated further.

In this model the primary fibril organization was based on the arcade model of Benninghoff (1925), which is valid in the central part of load bearing articular cartilage (Clark, 1991). Hence, care should be taken when using this model for other parts of the joint.

Essential parameters, including the thickness of the different zones, the collagen content and orientation in these zones and the distribution of the water content were not measured in the samples tested by DiSilvestro and Suh (2001). Therefore, these were obtained from other literature. A possible mismatch may account for part of the difference between model and experimental data. In the present model four primary fibril directions

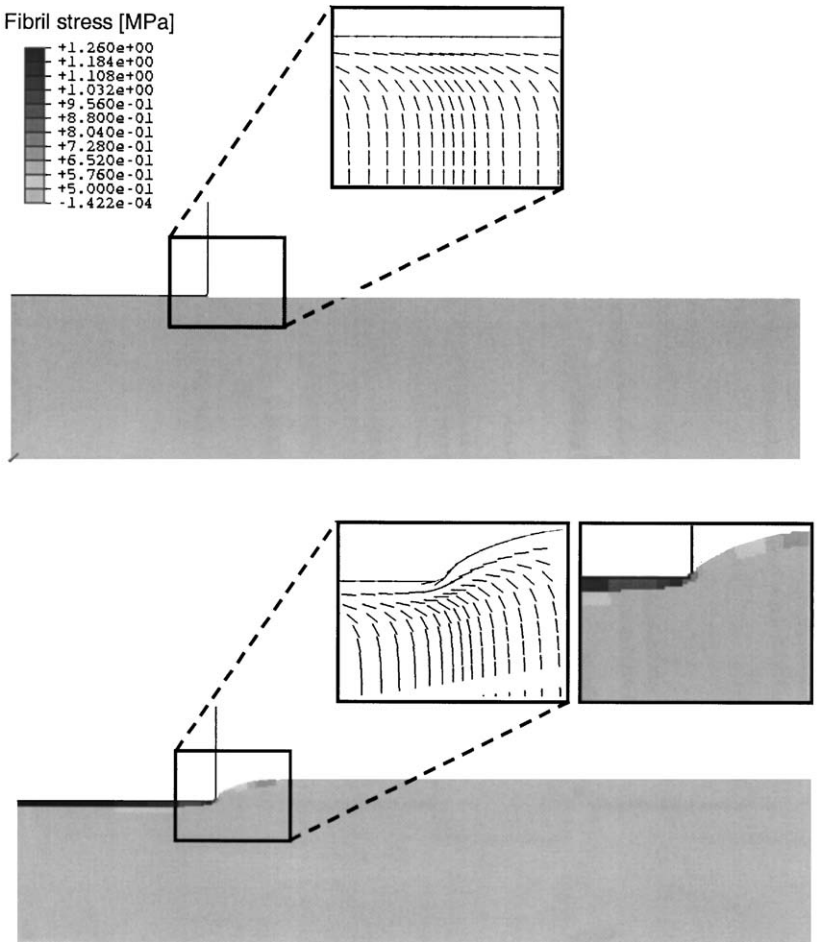


Fig. 9. Contour plot of the fibril stresses in the primary fibrils curving towards the center of the joint, along with the fibril directions around the edge of the indentor. At the top the unloaded state is shown and at the bottom the state at $t = 50$ s.

were included. This may appear a simplification of the actual fibril organization at the cartilage surface, but appropriate data that show otherwise is not available from the literature. This may account for part of the difference between model and experimental data.

The orientation of the secondary fibrils was assumed to be random. The structure of this network is not well known, but based on the data of Clark (1985, 1991) and SEM images of articular cartilage made by our own group, this assumption seems reasonable. Nevertheless, a possible mismatch could have occurred, which could account for part of the difference between model and experimental data.

It was assumed that the fibrils are not stressed during confined compression. However, based on the nodal nature of the fibrils and the inhomogeneous properties of the tissue, it is possible that local fibrils are placed in tension during unconfined compression. This could have resulted in a slight overestimation of the non-fibrillar-matrix stiffness. The stiffness of the fibrils was described separately in each integration point. This approach is valid, given the fact that the collagen fibrils are bonded to the non-fibrillar matrix, either by chemical bonds or entanglements (Junqueira and Carneiro, 1983).

In conclusion, a new poroviscoelastic fibril-reinforced cartilage model, including the complex arcade structure of the collagen network characteristic for articular cartilage, was developed. To the best of our knowledge this is the first poroviscoelastic fibril-reinforced cartilage model ever published. Also, it is the first cartilage model to incorporate the arcade structure of the collagen fibrils. It was demonstrated that with this model the deformation of the collagen fibrils, as well as their stresses and strains, can be calculated. It was also exhibited that fibrils at the same location can be stressed differently, depending on the architecture of the collagen network.

We conclude that the local stresses and strains in the articular cartilage are highly influenced by the local morphology of the collagen fibril network. We believe that to predict cartilage damage and adaptation the specialized collagen fibril-network morphology must be considered.

## Acknowledgements

This research was financially supported by the Dutch Organization for Scientific Research (ZonMw).

## References

Armstrong, C.G., Mow, V., Wirth, C., 1985. Biomechanics of impact-induced microdamage to articular cartilage—A possible genesis for chondromalacia patella. In: Finerman, G. (Ed.), AAOS Symposium on Sports Medicine: the Knee C. V. Mosby Co, St. Louis, pp. 70–84.

Atkinson, P., Haut, R., 1995. Subfracture insult to the human cadaver patellofemoral joint produces occult injury. Journal of Orthopaedic Research 13, 936–994.

Atkinson, T.S., Haut, R.C., Altiero, N.J., 1997. Fissuring of articular cartilage during blunt insult: An investigation of failure criteria. Transactions of Orthopaedic Research Society 22, 824.

Bank, R.A., Soundry, M., Maroudas, A., Mizrahi, J., TeKoppele, J.M., 2000. The increased swelling and instantaneous deformation of osteoarthritic cartilage is highly correlated with collagen degradation. Arthritis and Rheumatism 43, 2202–2210.

Benninghoff, A., 1925. Form und Bau der Gelenkknorpel in ihren Beziehungen zur Funktion. Zeitschrift fue Zellforschvly 2, 783–862.

Clark, J.M., 1985. The organization of collagen in cryofractured rabbit articular-cartilage—a scanning electron-microscopic study. Journal of Orthopaedic Research 3, 17–29.

Clark, J.M., 1991. Variation of collagen fibril alignment in a joint surface—a scanning electron-microscope study of the tibial plateau in dog, rabbit and man. Journal of Orthopaedic Research 9, 246–257.

DiSilvestro, M.R., Suh, J.K., 2001. A cross-validation of the biphasic poroviscoelastic model of articular cartilage in unconfined compression, indentation, and confined compression. Journal of Biomechanics 34, 519–525.

Donohue, J.M., Buss, D., Oegema Jr., T.R., Thompson Jr., R.C., 1983. The effects of indirect blunt trauma on adult canine articular cartilage. Journal of Bone and Joint Surgery, America 65, 948–957.

Durham, J., Shackleton, D.R., Billingham, M.F.J., Bitensky, L., Chayen, J., Muir, I.H, 1988. A reappraisal of the structure of normal canine articular cartilage. Journal of Anatomy 157, 89–100.

Garcia, J.J., Altiero, N.J., Haut, R.C., 1998. An Approach for Stress Analysis of Transversely Isotropic Biphasic Cartilage Under Impact Load. Journal of Biomechanical Engineering 120, 608–613.

Hasler, E.M., Herzog, W., Wu, J.Z., Muller, W., Wyss, U., 1999. Articular cartilage biomechanics: theoretical models, material properties, and biosynthetic response. Critical Review on Biomedical Engineering 27, 415–488.

Haut, R.C., Little, R.W., 1972. A constitutive equation for collagen fibers. Journal of Biomechanics 5, 423–430.

Hunziker, E., 1992. Articular artilage structure in humans and experimental animals. In: Kuettner, K.E., Peyron, J.G., Schleyer, R., Hascall, V.C. (Eds.), Articular Cartilage and Osteoarthritis. Raven Press, New York, pp. 183–199.

Junqueira, L.C., Carneiro, J., 1983. Basic Histology, 4th Edition. Lange Medical, Los Altos, p. 129.

Kääb, M.J., Ito, K., Clark, J.M., Notzli, H.P., 1998. Deformation of articular cartilage collagen structure under static and cyclic loading. Journal of Orthopaedic Research 16, 743–751.

Kääb, M.J., Ito, K., Rahn, B., Clark, J.M., Notzli, H.P., 2000. Effect of mechanical load on articular cartilage collagen structure: a scanning electron-microscopic study. Cells Tissues Organs 167 (2–3), 106–120.

Lai, W.M., Mow, V.C., Roth, V., 1981. Effects of nonlinear strain-dependent permeability and rate of compression on the stress behaviour of articular cartilage. Journal of Biomechanical Engineering 103, 61–66.

Lai, W.M., Hou, J.S., Mow, V.C., 1991. A triphasic theory for the swelling and deformation behaviors of articular cartilage. Journal of Biomechanical Engineering 113, 245–258.

Li, L.P., Soulhat, J., Buschmann, M.D., Shirazi-Adl, A., 1999. Nonlinear analysis of cartilage in unconfined ramp compression using a fibril reinforced poroelastic model. Clinical Biomechanics 14, 673–682.

Li, L.P., Buschmann, M.D., Shirazi-Adl, A., 2000. A fibril reinforced nonhomogeneous poroelastic model for articular cartilage: inhomogeneous response in unconfined compression. Journal of Biomechanics 33, 1533–1541.

Li, L.P., Shirazi-Adl, A., Buschmann, M.D., 2002. Alterations in mechanical behaviour of articular cartilage due to changes in depth varying material properties—a nonhomogeneous poroelastic model study. Computer Methods in Biomechanics and Biomedical Engineering 5, 45–52.

Lipshitz, H., Etheridge, R., Glimcher, M.J., 1975. In vitro wear of articular cartilage. Journal of Bone and Joint Surgery 57, 527–537.

Mak, A.F., 1986. The apparent viscoelastic behavior of articular cartilage—the contributions from the intrinsic matrix viscoelasticity and interstitial fluid flows. Journal of Biomechanical Engineering 108, 123–130.

Maroudas, A., 1976. Balance between swelling pressure and collagen tension in normal and degenerated cartilage. Nature 260, 808–809.

Mow, V.C., Guo, X.E., 2002. Mechano-electrochemical properties of articular cartilage: their inhomogeneities and anisotropies. Annual Review of Biomedical Engineering 4, 175–209.

Mow, V.C, Kuei, S.C., Lai, W.M., Armstrong, C.G., 1980. Biphasic creep and stress relaxation of articular cartilage in compression: theory and experiments. Journal of Biomechanical Engineering 102, 73–84.

Newberry, W.N., Zukosky, D.K., Haut, R.C., 1997. Subfracture insult to a knee joint causes alterations in the bone and in the functional stiffness of overlying cartilage. Journal of Orthopaedic Research 15, 450–455.

Pelletier, J.P., Martel-Palletier, J., Altman, R.D., Ghandur/Mnaymneh, L., Hower, D.S., Woessner, J.F., 1983. Collagenase and collagenolytic activity in human osteoarthritic cartilage. Arthritis and Rheumatism 26, 866–874.

Sanjeevi, R., Somanathan, N., Ramaswamy, D., 1982. A viscoelastic model for collagen fibres. Journal of Biomechanics 15, 181–183.

Schinagl, R.M., Gurskis, D., Chen, A.C., Sah, R.L., 1997. Depth-dependent confined compression modulus of full-thickness bovine articular cartilage. Journal of Orthopaedic Research 15, 499–506.

Silyn-Roberts, H., Broom, N.D., 1990. Fracture behaviour of cartilage-on-bone in response to repeated impact loading. Connective Tissue Research 24, 143–156.

Spilker, R.L., Suh, J.K., Mow, V.C., 1988. A finite element formulation of the nonlinear biphasic model for articular cartilage and hydrated sift tissues including strain-dependent permeability. In: Spilker, R.L., Simon, B.R. (Eds.), Computer Methods in Bioengineering. American Society of Mechanical Engineers, New York, pp. 81–92.

Thompson, R., Oegema, T., Lewis, J., Wallace, L., 1991. Osteoarthritic changes after acute transarticular load. Journal of Bone and Joint Surgery 73A, 990–1001.

Vener, J., Thompson Jr., R.C., Lewis, J., Oegema, T., 1992. Subchondral damage after acute transarticular loading: an in vitro model of joint injury. Journal of Orthopaedic Research 10, 759–765.

Verzijl, N., DeGroot, J., Zaken, C.B., Braun-Benjamin, O., Maroudas, A., Bank, R.A., Mizrahi, J., Schalkwijk, C.G., Thorpe, S.R.,

Baynes, J.W., Bijlsma, W.J., Lafeber, F.P.J.G., TeKoppele, J.W., 2002. Crosslinking by advanced glycation end products increases the stiffness of the collagen network in human articular cartilage. Arthritis and Rheumatism 46, 114–123.

Viidik, Q., 1968. A rheological model for uncalcified parallel-fibriled collagenous soft tissue. Journal of Biomechanics 1, 3–11.

van der Voet, A., 1997. A comparison of finite element codes for the solution of biphasic poroelastic problems. Proceedings of the Institute of Mechanical Engineering 211, 209–211.

Wang, J.L., Parnianpour, M., Shirazi-Adl, A., Engin, A.E., 1997. Failure criterion of collagen fiber: viscoelastic behavior simulated by using load control data. Theory and Application to Fracture Mechanics 27, 1–12.

Wilson, W., van Donkelaar, C.C., Ito, K., van Rietbergen, B., Huiskes, R., 2003. Pathways of load-induced cartilage damage causing cartilage degeneration in the knee after meniscectomy. Journal of Biomechanics 36, 845–855.